SANGOMA: Stochastic Assimilation for the Next Generation Ocean Model Applications EU FP7 SPACE-2011-1 project 283580

Deliverable 5.8:

Array analysis

Due date: 31/10/2015
Delivery date: 31/10/2015
Delivery type: Report , public

Jean-Marie Beckers Alexander Barth
Yajing Yan
University of Liège, BELGIUM

Peter Jan Van Leeuwen
University of Reading, UK

Lars Nerger
Alfred-Wegener-Institut, GERMANY

Arnold Heemink Nils van Velzen
Martin Verlaan
Delft University of Technology, NETHERLANDS

Pierre Brasseur Jean-Michel Brankart Adeline Bichet
CNRS-LGGE, FRANCE

Pierre De Mey
CNRS-LEGOS, FRANCE

Laurent Bertino
NERSC, NORWAY

Chapter 1

Introduction

This task aims to develop and test a methodology that allows to evaluate the performance of different observational arrays at detecting prior errors in an ensemble of simulations that is to be assimilated.

As an alternative to performing Observing System Simulations Experiments (OSSE), this tasks proposes to use two complementary approaches, that exploit existing, costly to perform, ensembles of simulations, and that allow to evaluate this performance without performing data assimilation. Instead, both approaches deal with observation-space view of prior errors, and exclude controllability. The first method, the ArM method, is part of the Sangoma toolbox (WP2), and represents the stochastic form of the Representer Matrix Spectrum described in Le Hénaff et al. (2009). The ArM approach features a simple criterion to characterize an observational array performance at detecting "prior" (forecast) errors. The second method, $tr(\mathbf{HK})$, is a new, alternative approach, that is both compatible and complementary with the ideas behind the ArM method. It uses a "posterior" approach, quantifying the impact that an observational array would have, if it was to be assimilated by the ensemble. Hence, whereas ArM is about how an array "views" the prior errors (it does not depend of a particular form of gain), $tr(\mathbf{HK})$ deals with observation-space gain, and thereby, with the effectiveness of the correction in observation space (it depends on the form of the gain). Note that unlike $tr(\mathbf{HK})$, the ArM method is not localized in the current form as it is meant for the assessment of localized arrays (mostly coastal), and can only be used in an ensemble-based approach.

After illustrating briefly the RMSpectrum/ArM method, we use $tr(\mathbf{HK})$ to evaluate the relevance of four observational networks (two satellites and two in situ measurements), given an assimilation system that uses the Ensemble Kalman filter (Evensen, 2003), and an ensemble that covers the North Atlantic and is designed to assimilate altimetric observations in the Gulf Stream region (Candille et al. 2015). We test the relevance of the four observational networks individually and together, on the free run as well as on the assimilated ensemble. We focus on the impact of assimilating sea surface height (SSH) as observed by two satellites, as well as temperature and salinity profiles (0-2000m) as observed in situ. Such an evaluation should allow a better understanding of the impact of different observational networks on an assimilation system, thereby leading to a better optimization in the future design of the observational networks to be assimilated. Note that the $tr(\mathbf{HK})$ method will be further developed in the Atlantos project.

The plan of the deliverable is as follows: chapter 2 briefly describes the RM-Spectrum/ArM approach, chapter 3 describes the $tr(\mathbf{HK})$ approach, chapter 4 describes the results from the $tr(\mathbf{HK})$ approach, and chapter 5 summarizes the conclusions that have been obtained from this work.

Chapter 2

The RMSpectrum/ArM approach

2.1 Method

RMSpectrum (“Representer Matrix Spectrum”) and ArM (“Array Modes”) are based on the very same ideas, but they differ by their implementation. In the RMSpectrum approach (Le Hénaff et al. 2009), the prior error covariance matrix can be of any origin, and the problem is solved in the form of an eigenspectrum problem. In the ArM approach (De Mey, 2014, pers.comm., available in the SANGOMA Tools), the prior errors are assumed to be approximated by a stochastic ensemble, and the problem becomes a simgular value problem. If the prior error covariance matrix is estimated by an Ensemble, both approaches yield the same answer, but the ArM approach is more efficient.

Details and examples of application of ArM in regional systems can be found in Lamouroux et al. (2015), in the WP2 documents and deliverables, and of course in the SANGOMA toolbox. The RMSpectrum approach is the one adopted below.

Although no data assimilation will be carried out here, we will use the unified notations of data assimilation as in Ide et al. (1997). Our initial question is whether one particular array $(\mathbf{H}, \mathbf{R})$ can be said to be “objectively satisfactory”, and whether, given two arrays, one of them can be said to be more efficient than the other (where $\mathbf{H}$ is the observational operator for that array, and $\mathbf{R}$ the covariance matrix of the associated observational error).

In the following, we use the following paradigm: a “good” array (regardless of its cost) is an array that can detect (and help correct) errors of a prior (pre-existing) estimate (be it from a model, a climatology, or a null estimate if nothing is known beforehand). The RMSpectrum approach consists of quantifying the number of degrees of freedom of “prior” errors which can be detected by an observational network.

Let us consider the Scaled Representer Matrix χ, expressed as follows:

$$\chi = \mathbf{R}^{-1/2}\mathbf{H}\mathbf{P}^{f}\mathbf{H}^{T}\mathbf{R}^{-1/2} \tag{2.1}$$

where $\mathbf{P}^f$ the covariance matrix of the prior (forecast) error. Hence, the Scaled Representer Matrix χ provides a way to compare the forecast error covariance matrix $\mathbf{P}^f$ in observation space with the observational error $\mathbf{R}$ covariance matrix (both can be full matrices). Comparing the eigenspectrum of χ with the eigenspectrum of the identity matrix allows to examine whether and under which circumstances an array will add information on top of prior knowledge, within the observational error. The spectra of χ is obtained via the diagonalization of χ as follow:

$$\chi = \mu\sigma\mu^T \tag{2.2}$$

where σ is a diagonal matrix containing the ordered eigenvalues λ of χ. Here, as written above, we are interested in the eigenvalues larger than 1, corresponding to detectable array modes on top of observational error. Each eigenvalue is associated with a distinct eigenmode in observation space, contained in the columns of μ. These modes exhibit the prior error patterns associated with each eigenvalue in observation space. To compare two networks, one computes the scaled representer matrix and associated spectra. The network with the largest number of eigenvalues above 1 can be defined as the objectively best network, in the sense that it is able to detect more of the scaled modes. However it is always necessary to qualify those formal comparisons by looking at state-space equivalents to the array modes. To that end, we compute the modal representers ρ, which can be seen as a matrix of representers for the array modes μ. The modal representer $\rho = \mathbf{P}^f\mathbf{H}^T\mathbf{R}^{-1/2}\mu$, whose columns contain the patterns associated with a scaled mode in the model state space, is obtained from equations (2.1) and (2.2) and orthonormality as defined below:

$$\mu^T\chi\mu = \mu^T\mathbf{R}^{-1/2}\mathbf{H}\mathbf{P}^f\mathbf{H}^T\mathbf{R}^{-1/2}\mu = \sigma \tag{2.3}$$

Here, σ appears as a rotated scaled representer matrix in the new basis defined by μ^T.

2.2 Implementation

Computing χ requires the knowledge of $\mathbf{P}^f$, $\mathbf{R}$, and $\mathbf{H}$. In theory, $\mathbf{P}^f$ has a very large number of entries (= number of state variables). For computational purposes, it is possible to select a reduced number of entries for $\mathbf{P}^f$ (reduced ranked approach). To avoid manipulating too large data, χ is computed following three steps: First, we directly compute $\mathbf{H}\mathbf{P}^f\mathbf{H}^T$ instead of $\mathbf{P}^f$, which is too costly to determine and too heavy to store. Then, we compute $\mathbf{R}^{-1/2}$, and finally χ. Because the matrix of modal representers $\rho = \mathbf{P}^f\mathbf{H}^T\mathbf{R}^{-1/2}\mu$ is also costly to compute, we select an arbitrary number of modes that we wish to examine.

2.3 Example

In this example we consider a single-variable 2D model with a prior error covariance matrix $\mathbf{P}^f$, and two observational networks: one triplet in the North-South (N-S) direction and the other triplet in the East-West (E-W) direction, with an error covariance matrix $\mathbf{R}$ that is diagonal and identical for both networks. Figure 2.1a shows the standard deviation of the prior error at the time and location of the two triplets, and Figure 2.1b shows the spatial correlation of prior errors. Whereas Figure 2.1a shows no apparent difference between both networks, Figure 2.1b shows that the error correlation scales are larger in the E-W direction. This directly affects the performances of the two networks, and translates into distinct scaled Representer Matrix Spectra (Figure 2.1c). According to Figure 2.1c, the N-S triplet is able to detect 3 degrees of freedom (3 eigenvalues higher than 1) whereas the E-W triplet (redundantly) constrains only 1 degree of freedom. This interpretation is confirmed by the associated three modal representers of each network (not shown), where modal representers 2 and 3 bring fresh information with respect to mode 1 in the case of the N-S network but not in the case of E-W network.

This simple example illustrates how the RMSpectrum approach allows to discriminate, in terms of detection and potential control of model state error structures, two networks with equal cost and seemingly equivalent return.

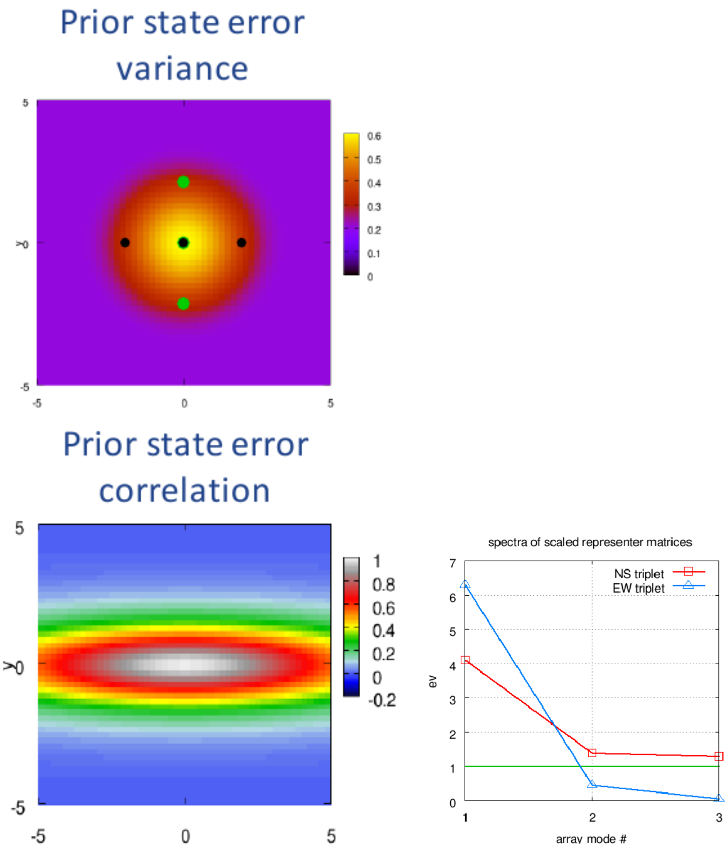

Figure 2.1: (a) Model sea level error standard deviation. Two observation networks are plotted: E-W network in black, and N-S network in green. The central point belongs to both. (b) Correlation in sea level error between the central point and the rest of the domain. (c) Scaled Representer Matrix Spectra of E-W (blue line) and N-S networks (red line). The green line is the spectrum of the identity matrix, equal to 1

Chapter 3

The $tr(\mathbf{HK})$ approach

3.1 Method

The $tr(\mathbf{HK})$ approach consists of quantifying the sensitivity of an ensemble to observations. In other words, how a given assimilation system uses the observations to “pull” the forecast signal from the background. This sensitivity is represented by the $\mathbf{HK}$ matrix, which compares the forecast error covariance matrix $\mathbf{P}^f$ (given by the stochastic ensemble) with the observational error covariance matrix $\mathbf{R}$. The $\mathbf{HK}$ matrix is obtained using the Ensemble Kalman filter (Evensen, 2003) assimilation method, assuming a Gaussian distribution. It is expressed as follows:

$$x^a = x^f + \mathbf{K}(y - \mathbf{H}x^f), \tag{3.1}$$

$$\text{with } \mathbf{K} = \mathbf{P}^f\mathbf{H}^T(\mathbf{H}\mathbf{P}^f\mathbf{H}^T + \mathbf{R})^{-1} \tag{3.2}$$

where x^a represents the assimilated state vector, x^f the background vector (simulated in the ensemble), y the observations, $\mathbf{H}$ the observational operator, $\mathbf{P}^f$ the covariance matrix of the forecast error, and $\mathbf{R}$ the covariance matrix of the observational error. Hence, the Kalman gain $\mathbf{K}$ weights the modifications brought by the observations to modify the background vector x^f, by comparing the forecast error $\mathbf{P}^f$ with the observational error $\mathbf{R}$. Included between 0 and 1, $\mathbf{K}$ increases with the amount of observation used to alter the background vector, that is to say, when the covariance matrix of observational error $\mathbf{R}$ is relatively smaller than the covariance matrix of the forecast error $\mathbf{P}^f$.

The gain in information brought by the observations is quantified via the computation of $tr(\mathbf{HK})$, which is the sum of the singular values of the $\mathbf{HK}$ matrix. Hence, $tr(\mathbf{HK})$ describes the number of useful, independent quantities in the observations (= degrees of freedom for signal) that are used to reduce the uncertainty of x^f, by quantifying how many degrees of freedom the observations are able to detect in $\mathbf{P}^f$. In other words, it evaluates which observational network detects most degree of freedom in the background vector x^f.

3.2 Implementation

As it was the case for the RMSpectrum/ArM approach, computing $tr(\mathbf{HK})$ requires the knowledge of $\mathbf{P}^f$, $\mathbf{R}$, and $\mathbf{H}$. In this sense, the two implementations are very efficient with most Sangoma methods. Here again, we use a reduced ranked approach for $\mathbf{P}^f$. We derive $\mathbf{P}^f$ from the 96-member ensemble described below and in Candille et al. (2015). In this example, $\mathbf{P}^f$ has therefore 96 entries. $\mathbf{H}$ is given by the observations, and $\mathbf{R}$ is chosen arbitrarily. To compute $tr(\mathbf{HK})$, we decompose $\mathbf{P}^f$ such as:

$$\mathbf{P}^f = \mathbf{S}^f {\mathbf{S}^f}^T, \tag{3.3}$$

$$\text{with } {\mathbf{S}^f}_{(i)} = ({x^f}_{(i)} - x^f)(m-1)^{-1/2} \tag{3.4}$$

where i corresponds to the individual ensemble members, and m to the total number of ensemble members. We can then rewrite $\mathbf{K}$ such as:

$$\mathbf{K} = \mathbf{S}^f [\mathbf{I} + \Gamma]^{-1} (\mathbf{HS}^f)^T \mathbf{R}^{-1} \tag{3.5}$$

$$\text{with } \Gamma = (\mathbf{HS}^f)^T \mathbf{R}^{-1} \mathbf{HS}^f = \mathbf{U} \Lambda \mathbf{U}^T \tag{3.6}$$

Therefore, **HK** can be expressed as:

$$\mathbf{HK} = \mathbf{HS}^f [\mathbf{I} + \Gamma]^{-1} (\mathbf{HS}^f)^T \mathbf{R}^{-1} \tag{3.7}$$

and $tr(\mathbf{HK})$ as:

$$tr(\mathbf{HK}) = tr[(\mathbf{I} + \Lambda)^{-1} \Lambda] = \Sigma(\lambda_k)(1+\lambda_k)^{-1}, \tag{3.8}$$

with λ_k = singular values of Γ

3.3 Data

The ensemble (Candille et al. 2015) is performed with the North Atlantic DRAKKAR configuration of NEMO version 3.4 (called NATL025) from January 1, 2005 to June 30, 2006. The horizontal resolution is 1/4°, which is considered eddy-permitting in the mid-latitudes. The forcing fluxes are calculated through bulk formulations using the ERA40 atmospheric forcing fields. The ensemble is built by introducing stochastic perturbations in the equation of state (Brankart 2013) after performing a single, non-perturbed integration from Levitus (1998) to January 1, 2005 to spin up the model state. Then, a 96-member ensemble of perturbed simulations is run for 6 months with the Brankart (2013) stochastic formulation, which is designed to spread mostly over areas with strong gradients and where the equation of state is strongly nonlinear such as in the Gulf Stream (region A in Figure 3.1). We thus expect an impact on the mesoscale circulation that is observed by altimetric data. Starting July 1, 2005, the ensemble is updated by a square root algorithm based on the SEEK (Singular Evolutive Extended Kalman) filter (Brasseur and Verron, 2006) for 12 months, assimilating altimetric data from

JASON-1 and ENVISAT. For this purpose, the compatibility between the ensemble and the observational error R for both satellites has been validated for R = 10 cm. This observational error standard deviation was tuned in the work of Candille et al. (2015) to optimize ensemble assimilation of altimetric observations. It is therefore important to keep in mind that this ensemble shows a spread mostly in the Gulf Stream region, and that its compatibility with observational errors has only been validated for SSH, with an error of 10 cm. It is beyond the scope of this study to assess the compatibility between the ensemble and the observational error for other values or variables.

To illustrate this ensemble, local time evolutions of the 96-member ensemble are shown in Figure 3.1, for 18 months (6 free run months and 12 assimilation months), in two different regions: Region A (68,5W; 35.5N) and B (38.75W; 45.5N). In the free run ensemble (cyan curve), the ensemble spread is larger and its saturation faster in the Region A, as compared to Region B. In the assimilated ensemble (green curves), the ensemble spread is reduced in both regions as compared to the free run ensemble.

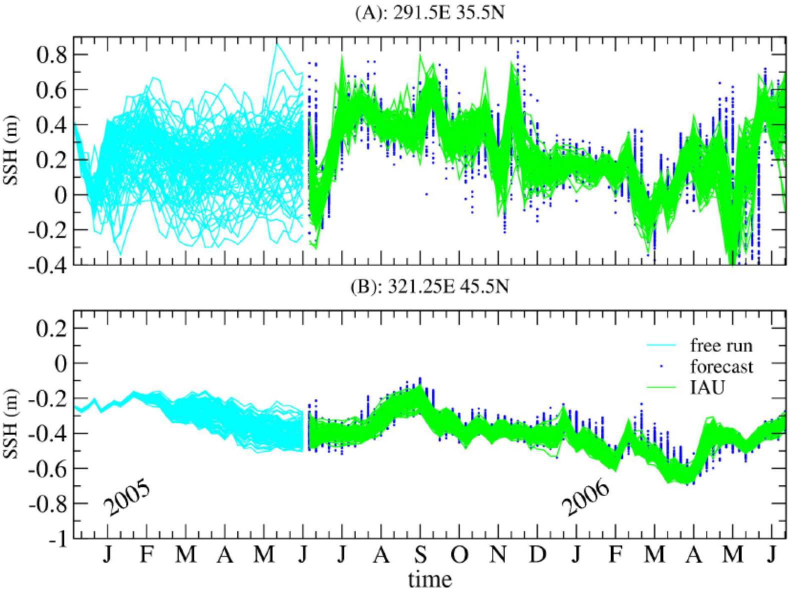

Figure 3.1: SSH time series of the ensemble (free run, forecast and assimilated) at two locations.

To illustrate the spatial representation of the ensemble, Figure 3.2 shows the ensemble mean (a-c) and ensemble standard deviation (d-f) of SSH, sea surface temperature (SST), and sea surface salinity (SSS), simulated in the free run ensemble for June 14, 2005. Figure 3.3 is identical to Figure 3.2 for June 14, 2006 but for the assimilated ensemble. According to Figure 3.2 (d-f), the ensemble spread in the free run ensemble is larger over the Gulf Stream for SSH (reaching 0.4 m in the southwest part), over the Gulf Stream, Labrador Current, and Denmark Straight for SST (reaching 1.8 °C in the northern side of the Gulf Stream), and over the Gulf Stream, Labrador Current, Denmark Straight, and the mouth of the Amazon and Mississippi rivers for SSS (reaching 1.25 psu in the Amazon mouth). As compared to the free run ensemble (Figure 3.2), the assimilated

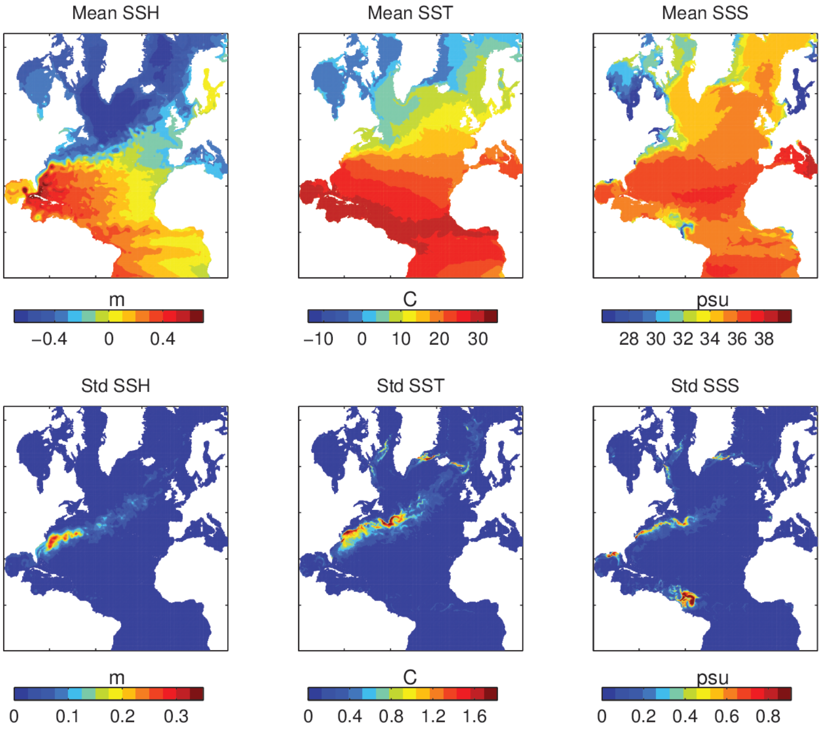

Figure 3.2: SSH, SST, and SSS as simulated in the free run ensemble mean (a-c) and as the ensemble standard deviation (d-f) for June, 14, 2005.

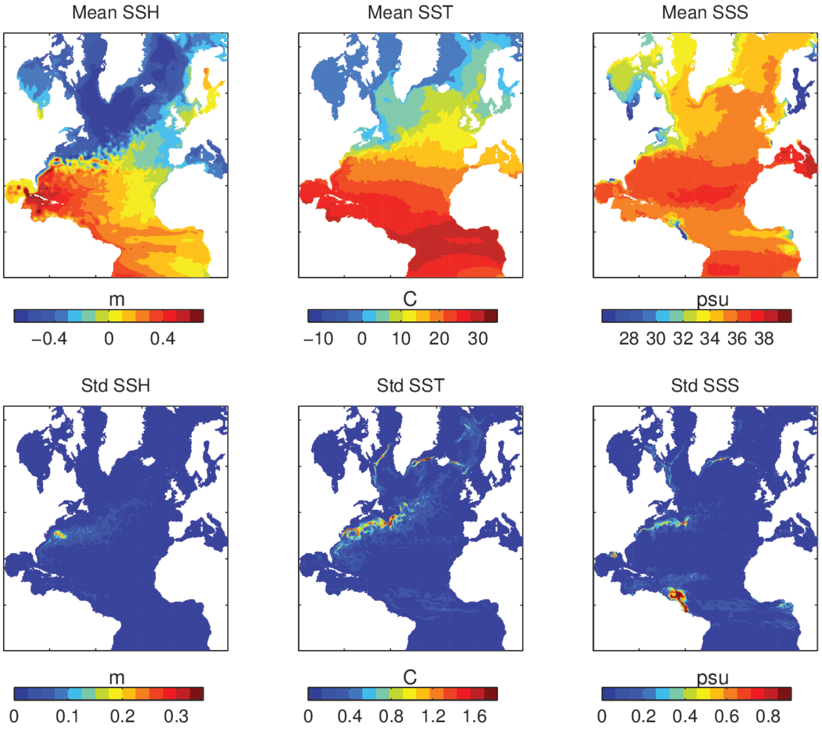

Figure 3.3: Same as Figure 3.2 in the assimilated ensemble for June, 14, 2006.

ensemble (Figure 3.3) is slightly more saline in the northern North Atlantic, and generally shows a smaller standard deviation, especially for SSH.

We evaluate four observational products. Along-track altimetric data (SSH) are taken from two satellites provided by AVISO-CNES: JASON-1 and ENVISAT. The JASON-1 mission has a 10-day cycle over 350 km inter-track distance at the equator, and the ENVISAT mission has a 35-day cycle over 80 km inter-track distance at the equator. Data for SST and SSS are taken from the ARGO profiles provided by the UK-MetOffice in addition to ship tracks (hereafter “ARGO”). The ARGO profiles are taken from an array of 3200 free-drifting profiling floats that measure the temperature and salinity of the upper 2000 meters of the ocean. They provide 100,000 temperature/salinity profiles and velocity measurements per year, distributed over the global oceans at an average 3-degree spacing. The floats cycle to 2000 meters depth every 10 days. We estimate the observational error (measurement and representativeness) associated with these observations to be comprised between 3 and 10 cm for SSH, 0.5 and 1 °C for the temperature profiles, and 0.1 and 0.2 psu for the salinity profiles. We do not account for the correlations of observational errors across the temperature and salinity profiles. We estimate a maximal observational window of 10 days around the date of interest, as we consider that the data recorded more than 5 days after the real date does not represent this date anymore.

To illustrate the observational space, Figure 3.4 is identical to Figure 3.2 but only shows location where data is observed, using a 10-day observational window from June, 9, 2005 to June, 19, 2005. Over this 10-day period, both satellite products show along-track data over the full domain, except north of 60N for JASON-1. In addition, JASON-1 shows a higher spatial resolution (Figure 3.4a) than ENVISAT (Figure 3.4b) because whereas JASON-1 has completed a full cycle in 10 days, this is not the case for ENVISAT, which needs 35 days to completes a full cycle. The ARGO surface data on the other hand shows isolated measurements (2135 measurements total including 1500 ARGO profiles for this 10-day window) located evenly across the domain, with a lack of measurements around the 10-20N band. Repeating the analysis using a 1-day observational window for June, 14, 2005 (not shown) shows that a lot of information is lost when reducing the observational window. We will therefore use a 10-day observational window for the remaining of the study.

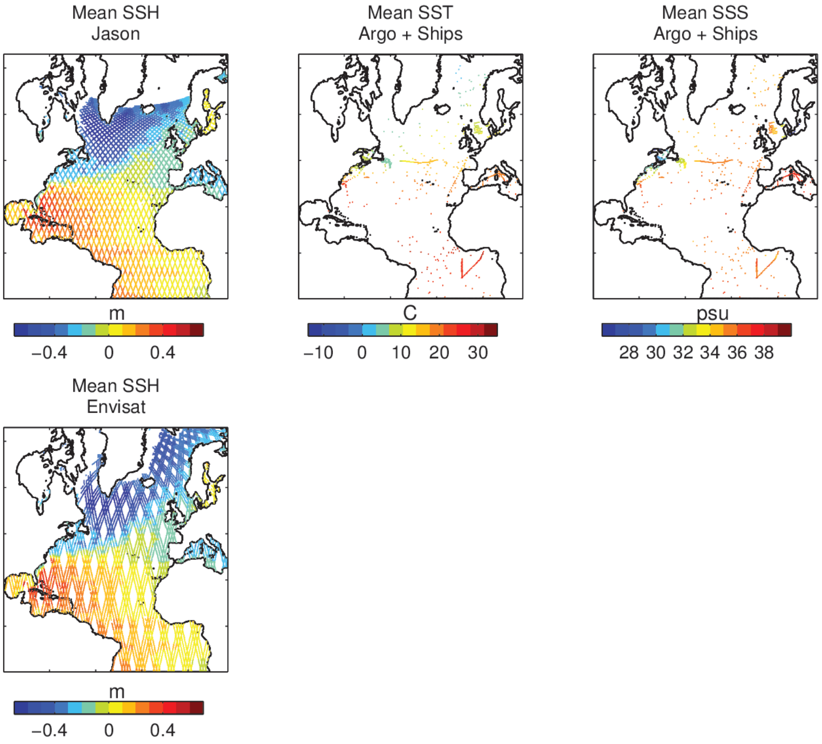

Figure 3.4: Same as Figure 3.2 but on the observational space, using a 10-day observational window from June 9, 2005 to June 19, 2005.

Chapter 4

Results

Because the Candillet et al. ensemble was not tested for its compatibility with all four observations evaluated here, we rather evaluate our results based on the sensitivity of $tr(\mathbf{HK})$ to divers parameters instead of providing quantitative conclusions on the observational networks.

4.1 Performance of assimilation system

First, we evaluate the performance of the assimilation system by computing $tr(\mathbf{HK})$ from the free run ensemble. Figure 4.1 evaluates the potential impact of assimilating SSH from JASON-1 (a), SSH from ENVISAT (d), temperature profiles from ARGO (b), and salinity profiles from ARGO (c), in the Candille et al. free run ensemble, using a 10-day observational window from June 9, 2005 to June 19, 2005. We use an observational error $\mathbf{R}$ of 3 cm for SSH, 0.5 °C for the temperature profiles, and 0.1 psu for the salinity profiles. According to Figure 4.1, $tr(\mathbf{HK})$ is higher over the Gulf Stream in all four cases, and additionally over the tropical Atlantic for ARGO. This indicates that in these regions, the forecast error ($\mathbf{P}^f$) is relatively larger than the observational error $\mathbf{R}$, and that consequently, the assimilation system acts to strongly alter the background vector x^f (= ensemble mean) with observations. We would like to recall at this point that the ensemble has not been validated for the assimilation of temperature and salinity profiles, and that consequently, Figures 6 (b-c) should be interpreted with care. Comparing Figure 4.1a with Figure 4.1d, we find that over this time period, both satellites bring a similar amount information to the ensemble, although the gain is spatially more homogeneous with JASON-1 than with ENVISAT, due its higher spatial resolution over this time period (see also Figure 3.2). Comparing Figure 4.1 (a and d) with Figure 4.1 (b-c), we find that although the satellite and in situ measurements bring most information over the Gulf Stream, the information brought by in situ measurements are more localized and more pronounced than the information brought by the satellites. Note also that ARGO brings additional information over the tropical Atlantic, but none north of 50N. We conclude that for the ensemble, time period, and observational errors chosen in this example, assimilating either of the four observational networks will improve the background vector over the Gulf Stream, extending over a more or less large area, depending on the observational network chosen (larger area but weaker signal with satellites). The comparison of Figure 3.2 (d-f) with Figure 4.1 indicates that $tr(\mathbf{HK})$ increases with the ensemble standard deviation ($\mathbf{P}^f$). This is not the case for the high values of $tr(\mathbf{HK})$ computed over the tropical Atlantic for temperature (Figure 3.4b) and salinity (Figure 3.4c), which instead, seem to result from a larger observational (ARGO) coverage (Figure 3.3).

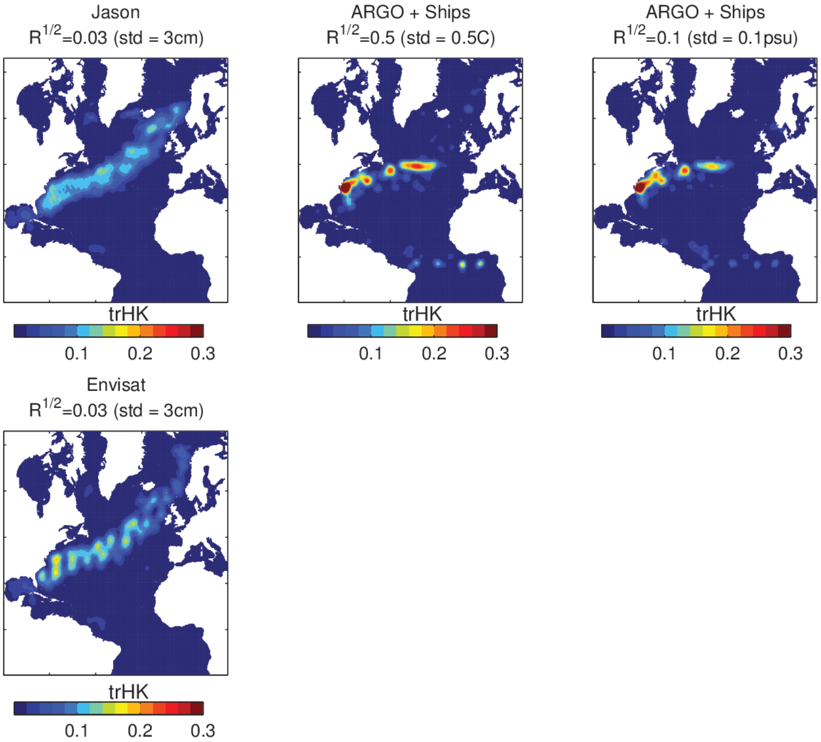

Figure 4.1: $tr(\mathbf{HK})$ computed from the free run ensemble (June 14, 2005) and SSH from JASON-1 (a), SSH from ENVISAT (b), temperature profiles from ARGO (c), and salinity profiles from ARGO (d), using a 10-day observational window from June 9, 2005 to June 19, 2005.

Repeating the analyze with a larger observational error $\mathbf{R}$ of 10 cm for SSH, 1 °C for temperature, and 0.2 psu for salinity (not shown), we find that $tr(\mathbf{HK})$ is roughly halved as compared to Figure 4.1. This indicates that the observational error $\mathbf{R}$ is a key factor influencing $tr(\mathbf{HK})$.

Figure 4.2a shows the potential impact of assimilating altimetric data from JASON-1 and ENVISAT at the same time. According to Figure 4.2a, assimilating both satellites roughly doubles the gain brought by observations. Figure 4.2b (c) shows the impact of assimilating altimetric data from JASON-1, ENVISAT and temperature (salinity) profiles from ARGO at the same time. Here, we find that $tr(\mathbf{HK})$ seems dominated by ARGO. However, because we know that the observational errors for temperature and salinity have not been optimized, we cannot conclude at this point, that ARGO brings more information than satellites. In addition, we also find that increasing the observational error $\mathbf{R}$ of ARGO increases the amount of information brought by the satellites (not shown). Therefore, we conclude that testing two observational networks in the Candille et al. ensemble via $tr(\mathbf{HK})$ cannot lead to a quantitative conclusion as long as the observational errors $\mathbf{R}$ are not optimized for all the observations prior to the analysis, because we find that $tr(\mathbf{HK})$ is very sensitive to $\mathbf{R}$.

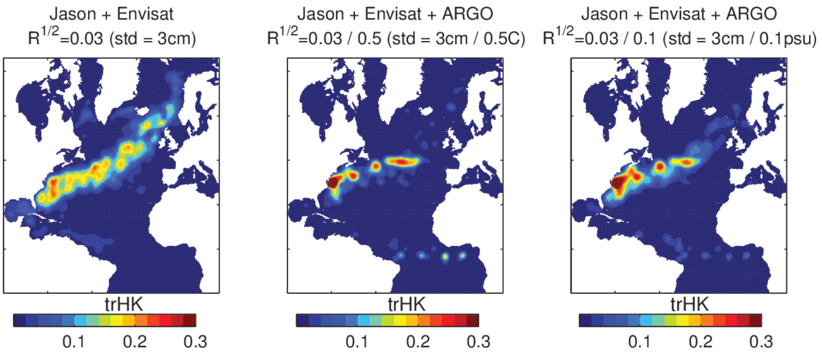

Figure 4.2: $tr(\mathbf{HK})$ computed from the freen run ensemble (June 14, 2005) and SSH from JASON-1 and ENVISAT (a), SSH from JASON-1 and ENVISAT and temperature profiles from ARGO (b), and SSH from JASON-1 and ENVISAT and salinity profiles from ARGO (c), using a 10-day observational window from June 9, 2005 to June 19, 2005.

4.2 Validation of assimilation system

We validate the assimilation system by computing $tr(\mathbf{HK})$ on the assimilated ensemble. Figure 4.3 evaluates the impact of potentially assimilating temperature (a) and salinity profiles from ARGO in the Candille et al. assimilated ensemble, using a 10-day observational window from June 9, 2006 to June 19, 2006. In other words, what would have happened if we had a third or fourth observation? As for Figure 4.1, we use a relatively small observational error R. According to Figure 4.3, assimilating the temperature or salinity profiles from ARGO, in addition to the altimetric data from JASON-1 and ENVISAT, only adds sporadic information along the Gulf Stream and tropical Atlantic. The lower values of $tr(\mathbf{HK})$ in Figure 4.3 (a-b) as compared to Figure 4.1 (b-c) indicate that less information is used from ARGO to modify the assimilated ensemble than to modify the free run ensemble. This suggests, in agreement with Figures 3.2 and 3.3, that the assimilated ensemble has a smaller forecast error than the free run ensemble, and that therefore, the assimilation system correctly reduces the forecast error, bringing the ensemble closer to the true state vector. Assimilating another observation at this point would only slightly improve the ensemble. This result also indicates that assimilated SSH improves the simulated temperature and salinity, which is encouraging.

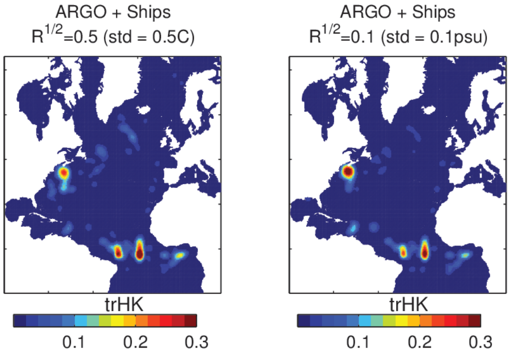

Figure 4.3: $tr(\mathbf{HK})$ computed from the assimilated ensemble (June 14, 2006) and the temperature profiles from ARGO (a), and salinity profiles from ARGO (b), using a 10-day observational window from June, 9, 2006 to June, 19, 2006.

Chapter 5

Conclusion

Using the $tr(\mathbf{HK})$ method, inspired from the Sangoma-tool ArM, itself a stochastic implementation of the RMSpectrum method (Le Hénaff et al. 2009), we show that the quantitative gain of information brought by an observational network depends mostly on 1) the observational error (the gain roughly doubles when observational error is halved) and 2) the forecast error (the gain increases with the forecast error). Qualitatively, the gain depends mostly on the location of the observations, and by extension, on the location of the forecast error: In our case, a lot of information is gained from observations over the Gulf Stream, because this is where the forecast error is largest. In our example, we conclude that the eddy-permitting model directly affects the performance of all four networks (satellite and in situ measurements), as a relatively higher $tr(\mathbf{HK})$ are found over the eddy-rich areas.

Our results also show that the gain of information brought by the satellite data is generally more numerous and spatially more homogeneous than ARGO, but that ARGO brings additional information over the tropical Atlantic. We also show that assimilating two satellites brings quantitatively twice as much information as assimilating only one satellite, and that assimilating ARGO data in addition to the two satellites does not add a lot more information than assimilating both satellite data. We would like to recall that while the quantitative results on SSH can be estimated reliable, this is not the case for the temperature and salinity profiles. Hence, the quantitative comparison between satellite and ARGO data should be taken with care, as $tr(\mathbf{HK})$ depends heavily on the observational error, which has been chosen arbitrarily and was not validated for temperature and salinity in the framework of our ensemble. In addition, we recall that the ensemble is especially designed to produce uncertainty in the SSH over the Gulf Stream, and not in other variables or regions.

Overall, we conclude that the $tr(\mathbf{HK})$ method has a relatively low computational cost, and is simple to implement and interpret. Although it shows promises, additional tests should be carried out to validate the ensemble with other observations than SSH and to better constrain the value of observational errors, prior drawing quantitative conclusions.

Chapter 6

References

Brankart J.-M., 2013. Impact of uncertainties in the horizontal density gradient upon low resolution global ocean modelling. it Ocean Modelling, **66**, 64–76.

Brasseur P. and Verron J., 2006. The SEEK filter method for data assimilation in oceanography: a synthesis, *Ocean Dynamics*, **56**, 650-661.

Candille G., Brankart J.-M., and Brasseur P., 2015. Assessment of an ensemble system that assimilates Jason-1/Envisat altimeter data in a probabilistic model of the North Atlantic ocean circulation. *Ocean Science*, **11**, 425-438.

Evensen G., 2003. The ensemble Kalman filter: Theoretical formulation and practical implementation. *Ocean Dynamics*, **53**, 343-367.

Kalman R.E., 1960. A New Approach to Linear Filtering and Prediction Problems. *Journal of Basic Engineering*, **82**.

Lamouroux, J., G. Charria, P. De Mey, S. Raynaud, C. Heyraud, P. Craneguy, F. Dumas, M. Le Hénaff, 2015: Assessment of RECOPESCA network contribution for the monitoring of 3D coastal model errors in the Bay of Biscay and the English Channel. Submitted to *Ocean Dynamics*.

Le Hénaff M., De Mey P., and Marsaleix P., 2009. Assessment of observational networks with the Representer Matrix Spectra method: application to a 3D coastal model of the Bay of Biscay. *Ocean Dynamics*, **59**, 3-20.

Levitus S. et al., 1998. World Ocean Database. NOAA Atlas NESDID 18, US Government Printing Office, Washington DC.